

Article

Variation Trend Analysis of Runoff and Sediment Time Series Based on the *R/S* Analysis of Simulated Loess Tilled Slopes in the Loess Plateau, China

Ju Zhang, Qingwu Hu , Shaohua Wang * and Mingyao Ai

School of Remote Sensing and Information Engineering, Wuhan University, No. 129, Luoyu Road, Wuhan 430079, China; zhangju@whu.edu.cn (J.Z.); huqw@whu.edu.cn (Q.H.); aimingyao@whu.edu.cn (M.A.)

* Correspondence: shwang@whu.edu.cn; Tel./Fax: +86-27-6877-8117

Received: 26 November 2017; Accepted: 21 December 2017; Published: 27 December 2017

Abstract: The objective of this study was to illustrate the temporal variation of runoff and sediment of loess tilled slopes under successive rainfall conditions. Loess tilled slopes with four microtopography types (straight cultivated slope, artificial backhoe, artificial digging, and contour tillage) under five slope gradients (5°, 10°, 15°, 20°, 25°) were simulated and a rainfall intensity of 60 mm/h was adopted. The temporal trends of runoff and sediment yield were predicted based on the Rescaled Range (*R/S*) analysis method. The results indicate that the Hurst indices of runoff time series and sediment time series are higher than 0.5, and a long-term positive correlation exists between the future and the past. This means that runoff and sediment of loess tilled slopes in the future will have the same trends as in the past. The results obtained by the classical *R/S* analysis method were the same as those of the modified *R/S* analysis method. The rationality and reliability of the *R/S* analysis method were further identified and the method can be used for predicting the trend of runoff and sediment yield. The correlation between the microtopography and the Hurst indices of the runoff and sediment yield time series, as well as between the slopes and the Hurst indices, were tested, and the result was that there was no significant correlation between them. The microtopography and slopes cannot affect the correlation and continuity of runoff and sediment yield time series. This study provides an effective method for predicting variations in the trends of runoff and sediment yield on loess tilled slopes.

Keywords: runoff; sediment; *R/S* analysis; Hurst index; loess tilled slopes

1. Introduction

The Loess Plateau is located in the northern part of China, covering the north of the Qinling Mt, south of the Yinshan Mt, west of the Taihang Mt, and east of the eastern edge of the Qinghai–Tibet Plateau (34°45′–39°40′N, 107°28′–111°15′E), with a total area of 62.68×10^4 km². Loess tableland, ridge, and hillock topographies are the basic topographical types of the Loess Plateau. The terrain is high in the northwest and low in the southeast. The terrain can be divided into high-mountain area (800–3000 m elevation), middle-mountain area (600–800 m elevation), and low-mountain area (400–600 m elevation) [1]. The total area of the land with slopes of more than 15 degrees is nearly 50%. Tilled slopes with slopes of more than 7 degrees account for 42.82% of the total cultivated land area [2], and are also serious erosion areas. Loess is the most widely distributed and the most developed quaternary sediment in the Loess Plateau, accumulation of which began about 240 million years ago and has extended to modern times. Affected by factors such as climate and altitude, the soil types in the Loess Plateau have obvious zonation patterns. Soil nutrients and water content are generally low and the soil is loose.

The Loess Plateau is located in mid-latitude inland, with continental monsoon climate characteristics. The northern and northwestern part of the region has a semi-arid monsoon climate type, while the southern part has a warm, temperate, semi-arid monsoon climate type. The annual precipitation is 150–750 mm, and precipitation is mostly concentrated in July to September, accounting for 60%–80% of the annual precipitation. Precipitation has the characteristics of uneven distribution and large variation in annual and seasonal distribution. Furthermore, there are a lot of rainstorms in the region, and the rainfall intensity of maximum rainstorms is above 120 mm/h. The soil erosion caused by them accounts for 60% of the total amount of soil and water loss in a year.

Land cover types of the Loess Plateau in 2008 are shown in Figure 1. It can be seen that cultivated land accounts for the largest proportion. The Loess Plateau is the oldest agricultural region in China. It is not only the first region in which agriculture took place in China, but also the region in which intensive agriculture has occurred for the longest. Nevertheless, nowadays, the Loess Plateau has a typical degraded eco-system, with the main problems being: the planting industry is dominated by the natural conditions, the utilization of resources is not enough; grassland degradation, desertification, and salinization are serious; agricultural production is unstable with low productivity [4]. One of the factors that cause these problems is the serious soil erosion in this region.

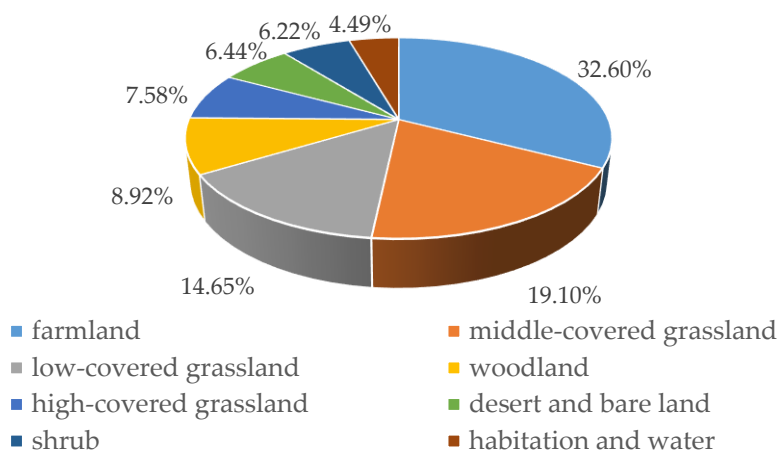


Figure 1. Land cover types of the Loess Plateau in 2008 (according to Zhou's research in 2016 [3]).

The Loess Plateau is the most serious soil and water loss area in the world. Over 60% of the land has been subjected to soil erosion. The area of soil erosion is $43 \times 10^4 \text{ km}^2$, including 138 counties. The area with serious soil erosion is $28 \times 10^4 \text{ km}^2$, and the area with particularly serious soil erosion is $10 \times 10^4 \text{ km}^2$. The soil erosion rate in most areas is between 5×10^3 and $2 \times 10^4 \text{ Mg km}^{-2}$ per year [5–7]. Soil erosion by water is the main type of erosion that causes soil and water loss on the Loess Plateau, which leads to the thinning of soil and a reduction in tilled land, and has directly affected local agricultural and industrial productivity. In addition, water erosion has caused river sediment deposition pollution, silting rivers, lakes, and reservoirs, for example, in the Yellow River, where 25% of the sediment load deposits along the riverbed, resulting in the riverbed rising 8–10 cm per year [5,8], threatening the lives and property of the people living along the lower reaches of the river.

In the past, many researchers have studied the laws of water erosion from different angles. Many studies have evaluated the effects of various land uses, cropping systems, soil management techniques, topography such as soil properties, land slopes, moisture content, rainfall intensity, climate, and differences in catchment responses on runoff and sediment losses based on field plot experiments [9–13]. Bryan and Poesen researched the interaction between slope length, seepage, and rill development based on rainfall simulation experiments [14]. Tayfur analysed the effects of the soil erodibility coefficients and exponents, and flow and loose soil depth on sediment discharge based on two-dimensional erosion processes and kinematic wave approximation [15]. Poulernard et al., in order to evaluate the effects

of land use (combustion and tillage) on the hydrodynamic characteristics of soil, carried out rainfall simulation tests at two different locations in northern Ecuador [16]. Zhang constructed an experiment in a hydraulic flume to examine the potential effects of sediment load on detachment rates and the assumed linear relationship between sediment load and detachment rate [17]. Shi et al. researched the soil erosion processes and sediment transport mechanisms of different degree slopes by twelve rainfall simulation experiments in a box, and found that the amount of contact sediment load is closely related to river sediment transport capacity [18]. In order to determine the correlation between the anti-erosion ability, surfaceness, and clay content of bare soils, Scherer concluded and parameterized a separation method based on a process erosion model, which balances simplicity and necessary process complexity [19]. Peter et al. analysed soil erosion in ravine collecting areas affected by land smoothing measures, based on rainfall simulation tests and UAV remote sensing data [20]. Abhinand Jha et al. used cosmogenic ^{7}Be as a tracer, and a diffusion-sorption model was presented, to estimate short-term soil loss rates after single and multiple rainfall tests [21]. The Universal Soil Loss Equation (USLE) has been widely used in predicting soil loss [22–26]. In summary, these papers mainly studied the influencing factors and modelled soil erosion, but conveyed little about the temporal variation of runoff and sediment on loess tilled slopes under successive rainfall conditions.

The variation of runoff and sediment under rainfall is a stochastic and fluctuating process, and there are limitations if the temporal variation of runoff and sediment on slopes is studied only from a linear or linear-like angle. To detect long-term dependence and self-similar time series, British hydrologist Hurst initially developed the Hurst index while studying non-standard behaviour in the Nile River. He calculated the Hurst index by Rescaled Range (R/S) Analysis [27]. The R/S Analysis, based on fractal theory, is an effective method to study the scale invariance of time series, and has been widely used in hydrological correlation studies. Mandelbrot, the founder of fractal theory, first studied the runoff time series model in 1981. He explained the Hurst phenomenon and extended Brownian motion to establish a fractional Brownian stochastic model to simulate annual runoff time series [28,29]. Hosking proposed the ARIMA model to simulate annual runoff processes [30], and the model has been applied broadly [31–35]. Tokinaga et al. combined fractal and Wavelet methods to predict temporal processes with fractal features [36], and this method was used to forecast the runoff of rivers such as the Songhua River, the Danube River, and the Pungwe River [37–40]. Szolgayova used R/S analysis and attempted to analyse the correlation between relevant influencing factors and long-term river flow [41]. The R/S Analysis method was used to analyse and predict variation of the runoff of rivers such as the Ter River, Fenhe River, Heihe River, Huai River, and seasonal rivers in the United Kingdom [42–46], and was also used to analyse and forecast climate variation tendencies [47–50]. The application of fractal research methods such as R/S analysis in hydrological research are mainly used to analyse long-term correlations of river runoff or to predict the runoff yield of a river; however, these methods are rarely used to analyse and predict the variation of runoff and sediment yield on slopes during rainfall.

In view of the above-mentioned facts, this study statistically analysed the runoff and sediment yield on loess tilled slopes with four microtopography types (artificial backhoe, artificial digging, contour tillage, and straight cultivated slope) under five slope gradients (5° , 10° , 15° , 20° , 25°) at each stage of rainfall. The trends of the runoff and sediment yield time series were analysed and predicted by the Rescaled Range Analysis method. The results indicate that runoff and sediment on loess tilled slopes in the future will have the same trends as those in the past. The results obtained by the classical R/S Statistic were tested by the modified R/S analysis method, which proved the rationality and reliability of the R/S analysis method in predicting trends of runoff and sediment yield. For the Loess Plateau, which is one of the most serious areas of water erosion in the world, this study can provide a scientific and theoretical basis for the monitoring and prevention of soil and water loss in the region to more effectively carry out soil and water conservation engineering and soil erosion control. At the same time, it further enriches the theory of the soil hydraulic erosion process model and promotes the development of soil erosion science.

2. Materials and Methods

In this paper, time series of runoff and sediment yields of different slopes were obtained by artificial rainfall simulation tests. Then, the Hurst index of each slope was obtained by the R/S Statistic to determine the temporal trends of runoff and sediment yield, and, subsequently, the effectiveness of the Hurst index was verified by an out-of-order test. The classical R/S Statistic that can calculate the non-periodic cycle length of the time series has some obvious shortcomings [51], so we used the modified R/S Statistic for the purpose of proving the rationality of the results obtained by the R/S analysis method. This study follows the framework outlined in Figure 2.

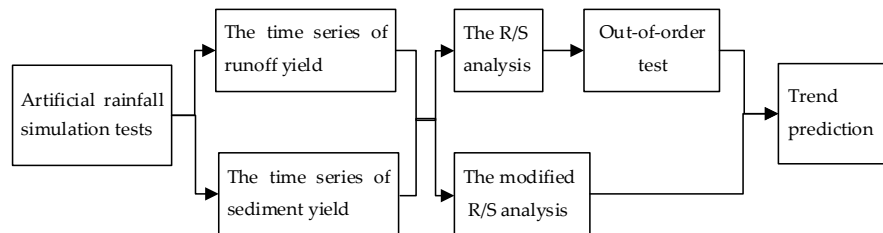


Figure 2. Framework for studying the variation in trends of runoff and sediment yield time series based on the R/S analysis method on loess tilled slopes.

2.1. Rescaled Range Analysis Method

2.1.1. Definition

Algorithms of R/S analysis are defined as follows [52–56].

1. Partition the length N time series into M equal sub-intervals $D_m (m = 1, 2, \dots, M)$ of length $n (2 \leq n < L)$, L is the length of the longest sub-interval, then $nM = N$, define each element in D_m as $p_{k,m} (k = 1, 2, \dots, n)$;
2. The mean of D_m is as follows:

$$e_m = \frac{1}{n} \sum_{i=1}^n p_{k,m} \quad (1)$$

3. In each interval D_m , the index of standard deviation S_{D_m} , series of cumulative mean deviation $\{x_{k,m}\}$, and range R_{D_m} are defined according to the following formulas

$$S_{D_m} = \sqrt{\frac{1}{n} \sum_{k=1}^n (p_{k,m} - e_m)^2} \quad (2)$$

$$x_{k,m} = \sum_{i=1}^k (p_{k,m} - e_m) \quad (3)$$

$$R_{D_m} = \max(x_{k,m}) - \min(x_{k,m}) \quad (4)$$

4. Compute the R/S Statistic for each interval and obtain the mean R/S Statistic for interval M , i.e.,

$$(R/S)_n = \frac{1}{M} \sum_{m=1}^M (R_{D_m} / S_{D_m}) \quad (5)$$

5. Mandelbrot found the following relationship through considerable research [57],

$$R_n / S_n = C \times n^H \quad (6)$$

where C is a constant and H is the Hurst index, ranging from 0 to 1. Take the common logarithm of both sides of Equation (6), i.e.,

$$\lg(R_n/S_n) = \lg C + H \lg n \quad (7)$$

6. Repeat step 1 to step 5, to obtain corresponding R_n/S_n values of different interval length n , then the least squares method is used in Formula (7) and the chart of double logarithm obtained and is the regression line slope.

The autocorrelation coefficient B is used to test the correlation of the time series.

$$B = 2^{2H-1} - 1; B \in [-0.5, 1] \quad (8)$$

When $H = 0.5$ and $B = 0$, the data variables in time series are independent random variables. When $H \neq 0.5$, the data variables in time series are non-random variables and have long-term correlations, and can be described by fractal Brownian motion. For $0 \leq H < 0.5$ and $-0.5 \leq B < 0$, it is shown that the future trend of the overall change violates the past, there exists an adverse state sustainability (negative correlation), and the adverse state sustainability gradually is enhanced with H approaching 0; $0.5 < H \leq 1$ and $0 < B \leq 1$, indicating that the future trend of the overall change is in line with the past, a state sustainability (positive correlation) exists, and the state is more persistent when H is closer to 1.

The fractal dimension D is used to evaluate the continuity of the time series.

$$D = 2 - H; D \in [1, 2] \quad (9)$$

The fractal features in the time series of runoff and sediment yield during rainfall are described quantitatively by D , i.e., the complexity of the temporal variations of runoff and sediment on different loess tilled slopes increases with D [58].

Meyer proposed an erosion–deposition mathematical model for soil erosion caused by rainfall and runoff, and proposed that the process should be extended to include the groundwater situation, vegetation status, microtopography, and surface water depth [59]. In this study, the soil erosion process model was extended to different microtopography formed by tillage and different slopes.

2.1.2. Out-of-Order Test

To determine whether the Hurst index is effective, the original time series can be randomly disordered to make the order of the original sequence completely different, and then the Hurst index H_2 of the random ordering series is calculated by the R/S Statistic and compared with the Hurst index of the original series, H_1 . If the original sequence is random, there is no difference between H_1 and H_2 . If the original sequence has a long-term correlation, then there will be a difference between H_1 and H_2 [60].

2.2. Modified R/S Analysis Method

Although the classical method can calculate the aperiodic cycle length of a time series, a Hurst index containing short-term memory, heterogeneity, or non-stationary time series is difficult to define clearly, and long-term correlation cannot be judged effectively. Lo et al. [61–63] modified the classical R/S analysis method, and introduced statistic V_n , and the formula is as follows:

$$V_n = (R_n/S_n)/\sqrt{n} \quad (10)$$

Substitute Formula (10) into Formula (6), i.e.,

$$V_n = (R_n/S_n)/\sqrt{n} = C \times n^{H-\frac{1}{2}} \quad (11)$$

When $H = 0.5$, V_n is a constant, the graph $V_n - \lg(n)$ shows a horizontal line, and the time series is random; when $0.5 < H \leq 1$, the graph $V_n - \lg(n)$ shows an upward trend; and when $0 \leq H < 0.5$, the curve $V_n - \lg(n)$ is downward. This method can be used to determine the rationality of the conclusions obtained by the classical R/S analysis method.

2.3. Experimental Facilities

The experimental soil was topsoil from a tilled slope in Yangling, Shaanxi. Yangling, in the Guanzhong area of Shaanxi Province, is south of the Loess Plateau. It has a typical continental climate and is in a semi-humid temperate zone. The average air temperature is 12.9 °C, annual precipitation is 630.9 mm, and summer precipitation accounts for more than 50% of annual precipitation. The main soil in the area is Lou Soil, which is formed on the basis of brown soil after long-term cultivation and a large amount of soil manure [64]. Although Lou Soil is not the most widely distributed soil in the Loess Plateau, the main cultivated soil in the area is mainly distributed in the southeastern part of the Loess Plateau, which is the main farming area in the Loess Plateau. The soil texture is silty loam, and the properties of the experimental soil are shown in Table 1.

The air-dried experimental soil was sifted through a sieve whose sieve pore diameter was 1 cm, and the water content of the soil approximately equaled 10%. The size of the soil-bin was 2.0 m × 1.0 m × 0.5 m, and its slope can be adjusted (Figure 3). There was a captation for collecting runoff and sediment at the bottom of the soil-bin.

The soil-bin was packed with sieved compacted soil according to layer, and there were 8 soil layers weighing 130 kg each. The bulk density of the tested soil was maintained at 1.30 g/cm³. Different farming measures were manually constructed in the soil-bin filled with soil, including artificial backhoe, artificial digging, contour tillage, and straight cultivated slope (Table 2, Figure 4). Among them, contour tillage was perpendicular to the slope direction to carry out horizontal farming on the slope, ridge height was 7–10 cm, and ridge distance was 30 cm; artificial backhoe was hoe farming in the traditional sense on the slope, and depth was 4–5 cm; artificial digging was digging the soil surface by hoe, depth was 5–8 cm, and distance was 20–25 cm; straight cultivated slope was smooth slope without any other measures.

Table 1. Properties of the experimental soil.

Soil Type	Soil Composition %			Soil Texture	Bulk Density g/cm ³	Water Content %	Organic Matter Content g/kg	Cation Exchange Capacity cmol/kg
	sand	silt	clay					
Lou Soil	2.82	55.74	41.44	silty loam	1.30	10	16.66	18.47

Table 2. To obtain different microtopography, different farming measures were manually constructed in the soil-bin filled with soil.

Microtopography	Measure	Height/Depth	Distance
Straight cultivated	smooth slope without any measure		
Contour tillage	horizontal farming	7–10 cm	30
Artificial backhoe	hoe farming	4–5 cm	
Artificial digging	digging	5–8	20–25



Figure 3. Simulated slopes under 5 degrees and 10 degrees (the air-dried tested soil was loaded into the soil-bins according to layer. The size of the soil-bin was 2.0 m × 1.0 m × 0.5 m, and its slope was adjustable. There was a captation for collecting runoff and sediment at the bottom of the soil-bin.).

Five slope gradients (5°, 10°, 15°, 20°, 25°) were simulated, and a side spray artificial rainfall machine was used for artificial rainfall at a height of 18 m. Rainfall evenness was more than 80%, and the effective rainfall area was 5 × 7 m². Soil erosion in the Loess Plateau is mainly caused by several heavy rainstorms, and heavy rainfall usually accounts for more than 60%, or even more than 90%, of total annual erosion [65]. According to the characteristics of rainfall in the Loess Plateau, a rainfall intensity of 60 mm/h was chosen. When runoff with sediment appeared at the outlet, the runoff time was recorded. Runoff and sediment were collected at intervals of two min after runoff was produced (Figure 5), and the rainfall lasted 90 min. Each test was repeated twice. The specific operation flow is shown in Figure 6. The runoff and sediment yield process curves of different slopes are shown in Figures 7 and 8 [66].

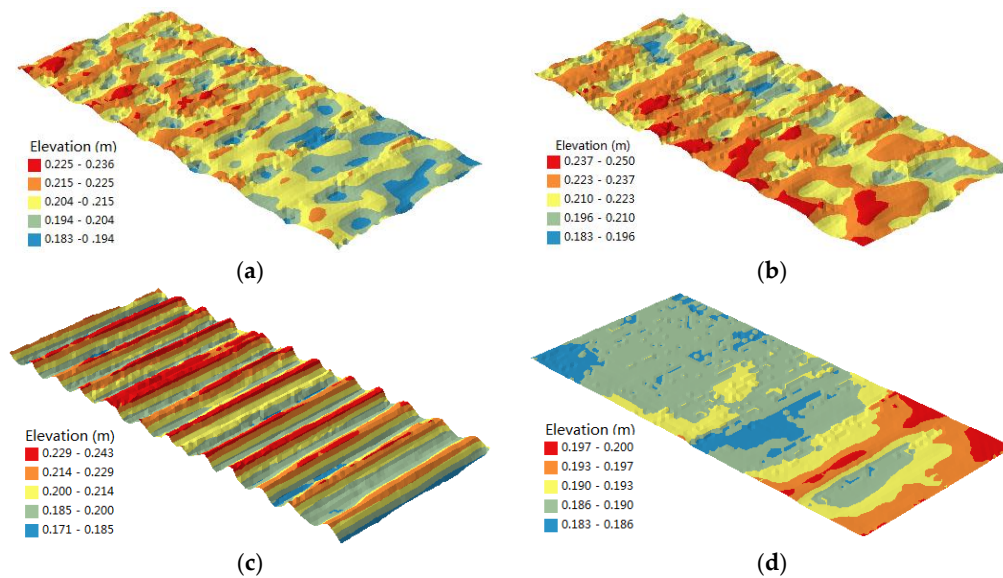


Figure 4. The different slopes were scanned by laser scanner, the laser spot cloud was obtained, and DEM(Digital Elevation Model) models of different slopes were obtained by kriging interpolation. (a) Artificial backhoe; (b) artificial digging; (c) contour tillage; (d) straight cultivated slope.



Figure 5. Runoff and sediment were collected at intervals of two min after runoff was produced. Water and sediment were separated by the static precipitation method.

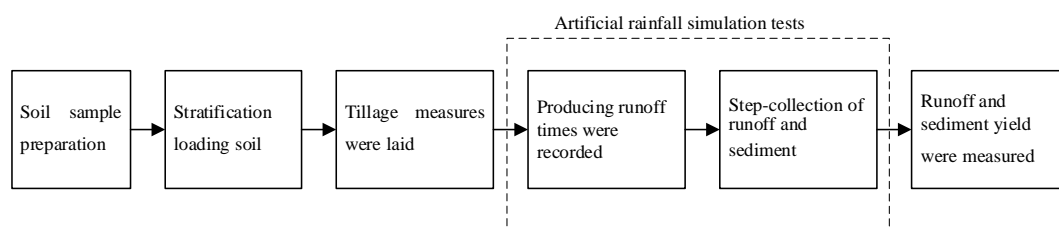


Figure 6. Steps for obtaining water and sediment at all stages of the artificial rainfall simulation tests.

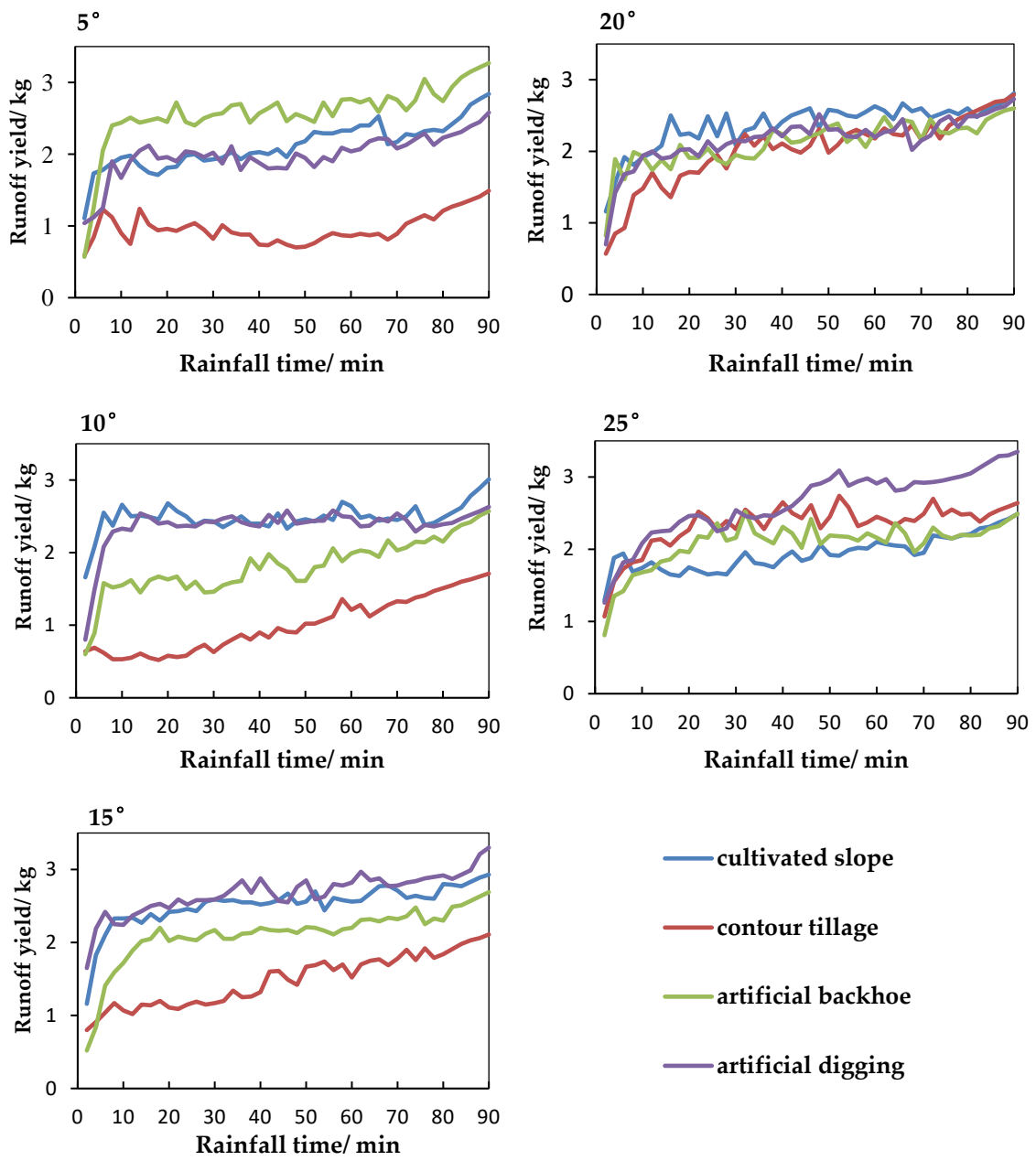


Figure 7. Runoff yield curves of different slopes (runoff was collected at intervals of two min after runoff was produced, and the rainfall lasted 90 min.).

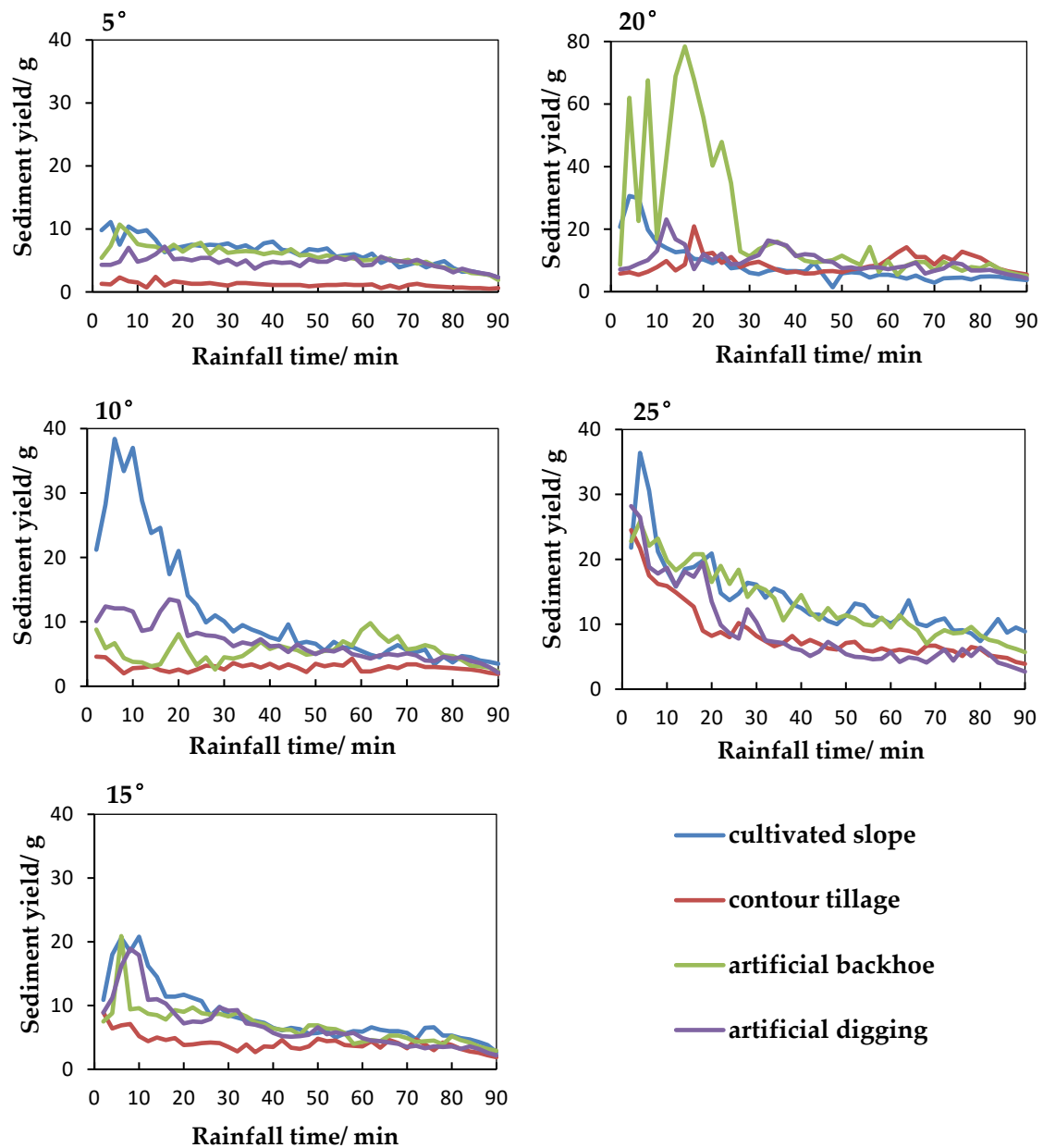


Figure 8. Sediment yield curves of different slopes (sediment was collected at intervals of two min after runoff was produced, and the rainfall lasted 90 min.).

3. Results

3.1. Long-Term Correlation of the Runoff Time Series

The duration of the rainfall experiment was 90 min and the water and sediment were collected at intervals of two min, thus the sample size N was 45. The runoff yield time series of five slopes and four microtopographies were analysed and the interval length n was $2 \leq n \leq N/2$. From Figure 9, we can see that $H \in [0.652, 0.869]$, $0 < B \leq 1$, and $1 \leq D < 1.5$, indicating that the time series of runoff yields exists in a persistent state (positive correlation). The time series of runoff yields were disrupted to create a random sequence, then the Hurst index of the random sequence was calculated. A Hurst index of the random sequence was obtained, $H \in [0.469, 0.611]$. In comparison, the Hurst index of the random sequence was obviously smaller than the original sequence, showing that the original time series of runoff yield was not a random sequence and had a long-term correlation. This proves that the

Hurst index was effective. The runoff hydrograph of different slopes can be seen in Figure 7; the runoff yield was fluctuant and increasing. $H > 0.5$, which indicates that the runoff yield will increase with rainfall time in the future.

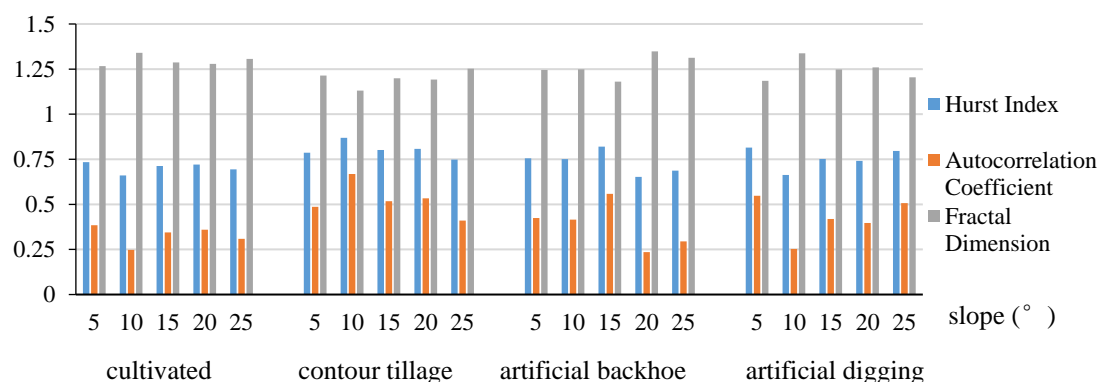


Figure 9. The Hurst index, autocorrelation coefficient, and fractal dimension of the runoff yield time series of different slopes based on the classical R/S analysis method.

The correlation between tillage and the Hurst index, and the correlation between the slope and the Hurst index were tested (Table 3), and the results were all irrelevant. Therefore, the Hurst index, the autocorrelation coefficient, and the fractal dimension of the runoff yield series with different microtopography are not significantly different or regular. It can be seen that microtopography cannot affect the correlation and continuity of the runoff yield time series. There is no correlation between the Hurst index, the autocorrelation coefficient, and the fractal dimension of the runoff series under different slopes. The slope is not the influencing factor in the continuity and correlation of the runoff yield time series.

Table 3. The correlation between microtopography and slope and the Hurst index, autocorrelation coefficient, and fractal dimension of the runoff yield time series.

		Hurst Index H	Autocorrelation Coefficient B	Fractal Dimension D
Microtopography	Correlation Coefficient	0.149	0.147	−0.149
	significance	0.530	0.536	0.530
Slope	Correlation Coefficient	−0.214	−0.217	0.214
	significance	0.366	0.358	0.366

The time series of runoff yield of the slopes with four microtopographies under five slopes were verified by modified R/S analysis (Figure 10), the result being all curves ($V_n - \lg(n)$) were increasing further, proving the rationality of the classical R/S analysis.

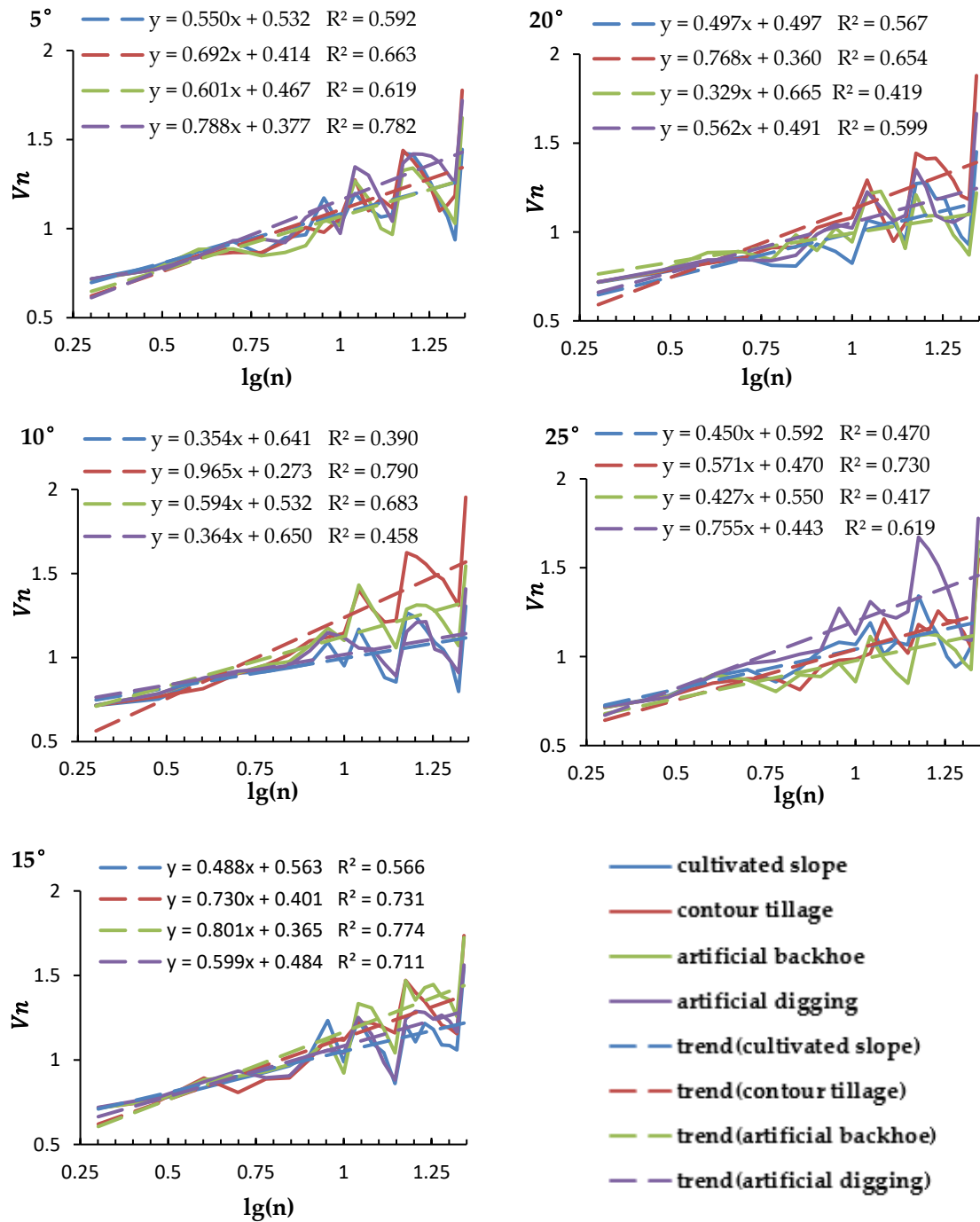


Figure 10. Modified R/S Statistic V_n testing of classical R/S analysis results of runoff yield time series at different slopes.

3.2. Long-Term Correlation of the Sediment Yield Time Series

The duration of the rainfall experiment was 90 min and the water and sediment were collected at intervals of two min, thus the sample size N was 45. The sediment yield time series of five slopes and four microtopographies were analysed and the interval length n was $2 \leq n \leq N/2$. From Figure 11, we can see that $H \in [0.627, 0.857]$, $0 < B \leq 1$, and $1 \leq D < 1.5$, indicating that the time series of sediment yield exists in a persistent state (positive correlation). The time series of sediment yield was disrupted to create a random sequence, then a Hurst index of the random sequence was calculated. A Hurst index of the random sequence was obtained, $H \in [0.482, 0.610]$. In comparison, the Hurst index of

the random sequence was obviously smaller than that of the original sequence, which shows that the original time series of sediment yield was not a random sequence and had a long-term correlation. This proves that the Hurst index is effective. The sediment hydrograph of different slopes can be seen in Figure 8, and with continuous rainfall, the sediment yield was fluctuant and decreasing. The sediment yield of the contour tillage slope was the least of the different slopes. H was greater than 0.5, which indicates that the sediment yield will increase with an increase in rainfall time in the future.

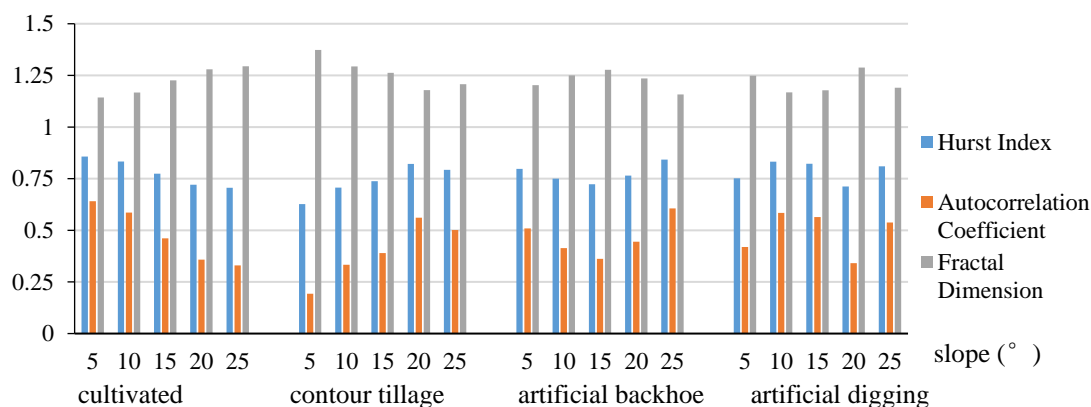


Figure 11. The Hurst index, autocorrelation coefficient, and fractal dimension of the sediment yield time series of different slopes based on the classical R/S analysis method.

The correlation between the microtopography and the Hurst index, and the correlation between the slope and the Hurst index were tested (Table 4), and the results were all significantly irrelevant. Therefore, the Hurst index, the autocorrelation coefficient, and the fractal dimension of the sediment yield series with different microtopographies are not significantly different or regular. It can be seen that microtopography cannot affect the correlation and continuity of the sediment yield time series. There is no correlation between the Hurst index, the autocorrelation coefficient, and the fractal dimension of the sediment series under different slopes. The slope is not the influencing factor in the continuity and correlation of the sediment yield time series.

Table 4. The correlation between microtopography, slope, and the Hurst index; autocorrelation coefficient; and fractal dimension of the sediment yield time series.

		Hurst Index H	Autocorrelation Coefficient B	Fractal Dimension D
Microtopography	Correlation Coefficient	0.117	0.111	−0.117
	significance	0.624	0.642	0.624
Slope	Correlation Coefficient	0.081	0.066	−0.081
	significance	0.733	0.783	0.733

The time series of sediment yield of the slopes with four microtopographies under five gradients were verified by modified R/S analysis (Figure 12), and all curves ($V_n - \lg(n)$) were increasing. This further proves the rationality of the classical R/S analysis.

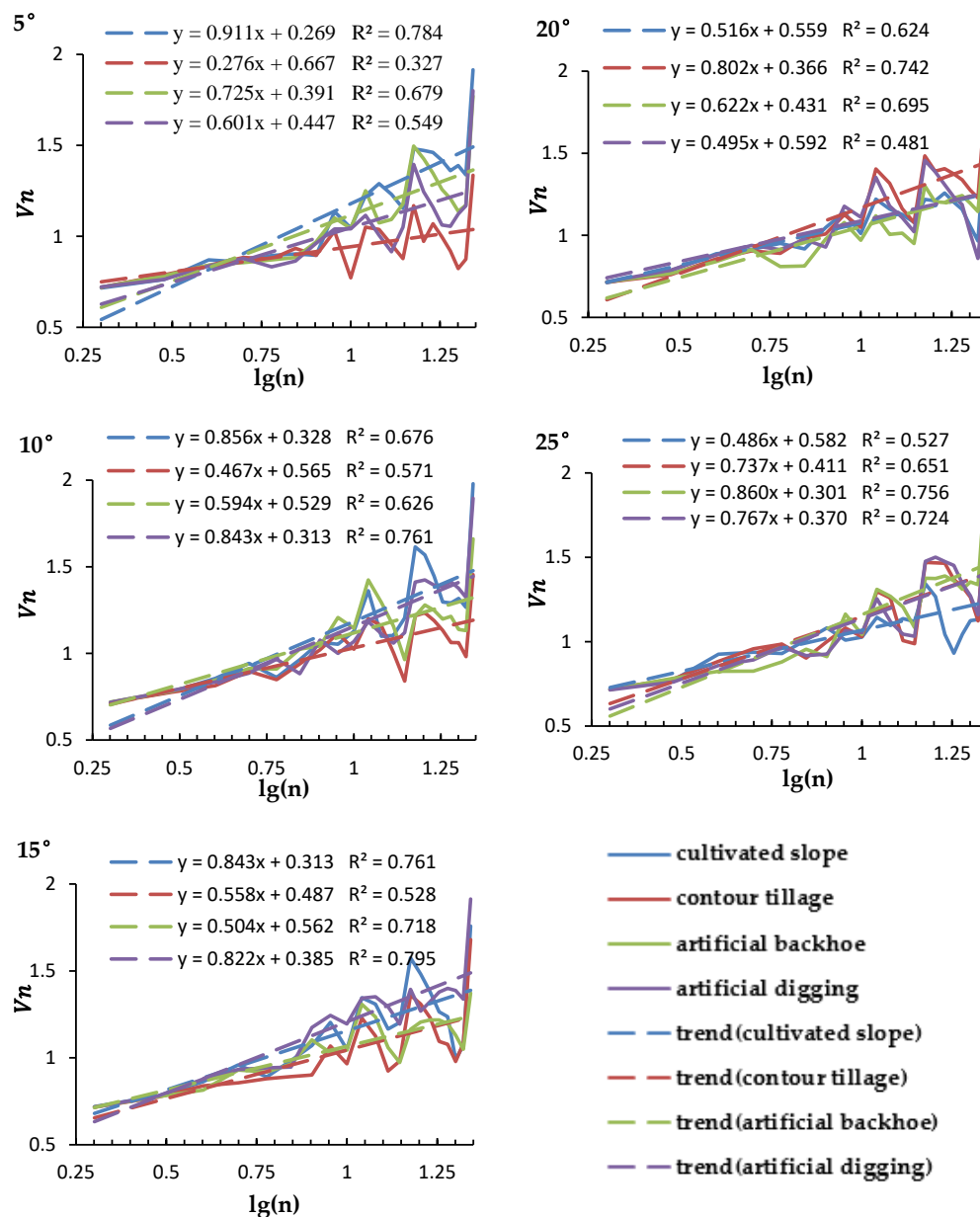


Figure 12. Modified R/S Statistic V_n testing of classical R/S analysis results of sediment yield time series at different slopes.

4. Discussion

The purpose of this study was to analyse the long-term correlation of runoff and sediment yield on loess slopes under rainfall conditions and to forecast a change in trend. In this study, the R/S analysis method was used for analysis. The duration of the rainfall experiment was 90 min and water and sediment were collected at intervals of two min, thus the sample size N was 45. The runoff and sediment time series of five slopes and four microtopographies were analysed, and the interval length n was $2 \leq n \leq N/2$. Using the modified R/S analysis method to test the results, it was proven that the results of the classical R/S analysis were rational.

From the results of the study, it is evident that the runoff and sediment yield time series of loess slopes with different slopes and different microtopographies have a long-term correlation; in the future, runoff will increase and sediment will decrease with an increase in rainfall time. Additionally, considering the theoretical study of soil erosion, the reason for this result may be because continuous

rainfall can lead to the development of a soil crust, so that soil runoff continues to increase. For sediment yield, when the rainfall hits the surface at the initiation of the rainfall, the surface soil is splashed and scattered, and sediment increases. With continuous rainfall, loose particles at the surface are transported. The erosion by rainfall on the slopes changes over time from splash erosion to surface erosion and even to rill erosion, resulting in redistribution of sediment particles and a reduced sediment output. In addition, splash brakes the loose particle structure of the surface soil and forms a soil crust, so that the adhesion of the surface soil particles increases [18], hindering the ability of rainfall to move the soil particles, resulting in a reduction in sediment yield.

The effects of microtopography and slope on long-term correlation were examined when the long-term correlation between soil runoff and sediment yield was studied. The results showed that microtopography and slope are not influencing factors on the long-term correlations of runoff and sediment yield. The effect of the long-term correlations of soil runoff and sediment yield can also be extended to aspect, rainfall intensity, vegetation status, soil type, and so on.

The experimental soil tested in this study was Lou soil, which is the main cultivated soil in the southern Loess Plateau. The soil types in the Loess Plateau also include loessial soil, dark loessial soil, lime soil, and cinnamon soil. The long-term correlation of runoff and sediment yield on these types of soils under rainfall conditions remains to be studied. In addition, in this study, the rainfall process was simulated by an artificial rainfall experiment; the soil condition and the rainfall environment were single and fixed, but in the actual field environment, the soil structure, soil composition, rainfall parameters, and other conditions are more complicated, so the simulation and prediction of the runoff and sediment yield time series of slopes in the Loess Plateau area should be further studied.

Even though microtopography and slope cannot affect the correlation and continuity of runoff and sediment yield time series, it can be seen from Figures 7 and 8 that runoff and sediment of the gentle slope and the contour tillage conditions are obviously less. Hence, the farmland should be reused for other purpose in areas where steep slopes are numerous and soil erosion is serious. Cultivation should be carried out in a way of retarding the gradient of slope cultivation in the Loess Plateau.

5. Conclusions

In this paper, the characteristics of runoff and sediment yield under different microtopographies on the Loess Plateau are studied, and the trend of water and sediment time series were analysed by the R/S analysis method.

From the results of the runoff and sediment yield time series based on the R/S analysis method, the Hurst indices are all greater than 0.5, so they have a long-term correlation; in the future, variation in trends of runoff and sediment yield will be the same as in the past. The difference is that runoff increases and sediment yield decreases with an increase in rainfall time. The results obtained by classical R/S analysis were tested by the modified R/S analysis method, which proved their rationality.

The correlations between the microtopography, the slope, and the Hurst index of the runoff and sediment yield time series were tested, and the result was that there is no significant correlation between them. Therefore, microtopography and slope cannot affect the correlation and continuity of runoff and sediment yield time series.

This study's prediction of variations in trends of runoff and sediment yield on loess tilled slopes under certain rainfall conditions via the R/S analysis method is reasonable and scientific. As a mathematical statistical method, the R/S analysis method cannot reveal the internal process of runoff and sediment formation on loess tilled slopes from the soil erosion level. It is suggested to combine the R/S analysis method and the soil hydrological model based on the soil erosion mechanism to simulate and forecast the runoff and sediment yield on loess tilled slopes in the Loess Plateau, to more effectively prevent soil erosion.

Acknowledgments: This work was supported by National High-tech R&D Program of China (863 Program) (Grand No.2013AA102401) and National Key Research Program(Grant No.2016YFF0103502). We appreciate Professor Shenghui Fang for the kind assistance in data analysis.

Author Contributions: Qingwu Hu and Shaohua Wang conceived and designed the experiments; Ju Zhang and Mingyao Ai performed the experiments; Ju Zhang analyzed the data; Huqing Wu and Ju Zhang contributed reagents/materials/analysis tools; Ju Zhang and Qingwu Hu wrote the paper.

Conflicts of Interest: The authors declare no conflict of interest.

References

1. Yang, W.Z.; Shao, M.A. *Research on Soil Moisture in the Loess Plateau*; Science Press: Beijing, China, 2000; pp. 4–9. (In Chinese)
2. Peng, W.Y.; Zhang, K.L.; Liu, L. Land Gradient and Reclamation Ratio on Loess Plateau Based on GIS. *J. Soil Water Conserv.* **2001**, *15*, 33–36. (In Chinese)
3. Zhou, S.; Shao, Q.; Cao, W. Characteristics of Land Use and Land Cover Change in the Loess Plateau over the Past 20 Years. *J. Geo-Inform. Sci.* **2016**, *18*, 190–199. (In Chinese)
4. Wang, Z.; Zhang, B. Ecological restoration and reconstruction and agriculture sustainable development in loess plateau of Northwest China. *Syst. Sci. Compr. Stud. Agric.* **2003**, *19*, 112–115. (In Chinese)
5. Fu, B.J.; Zhao, W.W.; Chen, L.D.; Zhang, Q.J.; Lü, Y.H.; Gulnick, H.; Poesen, J. Assessment of soil erosion at large watershed scale using RUSLE and GIS: A case study in the Loess Plateau of China. *Land Degrad. Dev.* **2005**, *16*, 73–85. [[CrossRef](#)]
6. Chen, L.; Wei, W.; Fu, B.; Lu, Y. Soil and Water Conservation on the Loess Plateau in China: Review and Perspective. *Progress Phys. Geogr.* **2007**, *31*, 389–403. [[CrossRef](#)]
7. Ping, Z.; Wen, A.; Zhang, X.; He, X. Soil conservation and sustainable eco-environment in the Loess Plateau of China. *Environ. Earth Sci.* **2013**, *68*, 633–639. [[CrossRef](#)]
8. Ping, Z.; Wen, A.; Zhang, X.; He, X. Soil and water loss from the Loess Plateau in China. *J. Arid Environ.* **2000**, *45*, 9–20.
9. Kang, S.; Zhang, L.; Song, X.; Zhang, S.; Liu, X.; Liang, Y.L.; Zheng, S.Q. Runoff and sediment loss responses to rainfall and land use in two agricultural catchments on the Loess Plateau of China. *Hydrol. Process.* **2001**, *15*, 977–988. [[CrossRef](#)]
10. Bissonnais, Y.L.; Renaux, B.; Delouche, H. Interactions between soil properties and moisture content in crust formation, runoff and interrill erosion from tilled loess soils. *Catena* **1995**, *25*, 33–46. [[CrossRef](#)]
11. Ziadat, F.M.; Taimeh, A.Y. Effect of rainfall intensity, slope, land use and antecedent soil moisture on soil erosion in an arid environment. *Land Degrad. Dev.* **2013**, *24*, 582–590. [[CrossRef](#)]
12. Keesstra, S.; Pereira, P.; Novara, A.; Brevik, E.C.; Azorin-Molina, C.; Parras-Alcántara, L.; Jordánh, A.; Cerdà, A. Effects of soil management techniques on soil water erosion in apricot orchards. *Sci. Total Environ.* **2016**, *551*, 357–366. [[CrossRef](#)] [[PubMed](#)]
13. Pal, I. *Rainfall Trends in India and Their Impact on Soil Erosion and Land Management*; University of Cambridge: Cambridge, UK, 2010.
14. Bryan, R.B.; Poesen, J. Laboratory experiments on the influence of slope length on runoff, percolation and rill development. *Earth Surf. Proc. Land.* **1989**, *14*, 211–231. [[CrossRef](#)]
15. Tayfur, G. Modeling Two-Dimensional Erosion Process over Infiltrating Surfaces. *J. Hydrol. Eng.* **2001**, *6*, 259–262. [[CrossRef](#)]
16. Poulénard, J.; Podwojewski, P.; Janeau, J.L.; Collinet, J. Runoff and soil erosion under rainfall simulation of Andisols from the Ecuadorian Páramo: Effect of tillage and burning. *Catena* **2001**, *45*, 185–207. [[CrossRef](#)]
17. Zhang, G.H.; Liu, Y.M.; Han, Y.F.; Zhang, X.C. Sediment transport and soil detachment on steep slopes: II. Sediment feedback relationship. *Soil Sci. Soc. Am. J.* **2009**, *73*, 1298–1304. [[CrossRef](#)]
18. Shi, Z.H.; Fang, N.F.; Wu, F.Z.; Wang, L.; Yue, B.J.; Wu, G.L. Soil erosion processes and sediment sorting associated with transport mechanisms on steep slopes. *J. Hydrol.* **2012**, *454*, 123–130. [[CrossRef](#)]
19. Scherer, U.; Zehe, E.; Träbing, K.; Kai, G. Prediction of soil detachment in agricultural loess catchments: Model development and parameterisation. *Fuel Energy Abstr.* **2012**, *90*, 63–75. [[CrossRef](#)]
20. Peter, K.D.; D’Oleire-Oltmanns, S.; Ries, J.B.; Marzolf, I.; Hssaine, A.A. Soil erosion in gully catchments affected by land-levelling measures in the Souss Basin, Morocco, analysed by rainfall simulation and UAV remote sensing data. *Catena* **2014**, *113*, 24–40. [[CrossRef](#)]

21. Jha, A.; Schkade, U.; Kirchner, G. Estimating short-term soil erosion rates after single and multiple rainfall events by modelling the vertical distribution of cosmogenic ^7Be in soils. *Geoderma* **2015**, *243*, 149–156. [[CrossRef](#)]
22. Wischmeier, W.H.; Smith, D.D. Predicting rainfall erosion losses—a guide to conservation planning. *Agric. Handbook* **1978**, *537*, 285–291.
23. Mihara, M.; Yamamoto, N.; Ueno, T. Application of USLE for the prediction of nutrient losses in soil erosion processes. *Paddy Water Environ.* **2005**, *3*, 111–119. [[CrossRef](#)]
24. Class, S. Application of USLE Model & GIS in Estimation of Soil Erosion for Tandula Reservoir. In Proceedings of the 43rd International Symposium on Agricultural Engineering, Actual Tasks on Agricultural Engineering, Opatija, Croatia, 24–27 February 2015.
25. Ali, S.A.; Hagos, H. Estimation of soil erosion using USLE and GIS in Awassa Catchment, Rift valley, Central Ethiopia. *Geoderma Reg.* **2016**, *7*, 159–166. [[CrossRef](#)]
26. Rizeei, H.M.; Saharkhiz, M.A.; Pradhan, B.; Ahmad, N. Soil erosion prediction based on land cover dynamics at the Semenyih watershed in Malaysia using LTM and USLE models. *Geocarto Int.* **2016**, *31*, 1158–1177. [[CrossRef](#)]
27. Hurst, H.E.; Black, R.P.; Simaika, Y.M. *Long-Term Storage: An Experimental Study*; Constable: London, UK, 1965.
28. Mandelbrot, B.B.; Wheeler, J.A. The Fractal Geometry of Nature. *Q. Rev. Biol.* **1983**, *147*, 468. [[CrossRef](#)]
29. Mesa, O.J.; Poveda, G. The Hurst effect: The scale of fluctuation approach. *Water Resour. Res.* **1993**, *29*, 3995–4002. [[CrossRef](#)]
30. Hosking, J.R.M. Modeling persistence in hydrological time series using fractional differencing. *Water Resour. Res.* **1984**, *20*, 1898–1908. [[CrossRef](#)]
31. Valipour, M. Long-term runoff study using SARIMA and ARIMA models in the United States. *Meteorol. Appl.* **2015**, *22*, 592–598. [[CrossRef](#)]
32. Kumar, S.V.; Vanajakshi, L. Short-term traffic flow prediction using seasonal ARIMA model with limited input data. *Eur. Transp. Res. Rev.* **2015**, *7*, 21. [[CrossRef](#)]
33. Soni, K.; Kapoor, S.; Parmar, K.S.; Kaskaoutis, D.G. Statistical analysis of aerosols over the Gangetic–Himalayan region using ARIMA model based on long-term MODIS observations. *Atmos. Res.* **2014**, *149*, 174–192. [[CrossRef](#)]
34. Peng, Y.; Lei, M.; Li, J.B.; Peng, X.Y. A novel hybridization of echo state networks and multiplicative seasonal ARIMA model for mobile communication traffic series forecasting. *Neural Comput. Appl.* **2014**, *24*, 883–890. [[CrossRef](#)]
35. Bari, S.H.; Rahman, M.; Hussain, M.; Ray, S. Forecasting monthly precipitation in Sylhet city using ARIMA model. *Civ. Environ. Res.* **2015**, *7*, 69–77.
36. Tokinaga, S.; Moriyasu, H.; Miyazaki, A.; Shimazu, N. Forecasting of time series with fractal geometry by using scale transformations and parameter estimations obtained by the wavelet transform. *Electr. Commun. Jpn.* **1997**, *80*, 20–30. [[CrossRef](#)]
37. Uamusse, M.M.; Ndalila, P.; Júliotsamba, A.; De, F.; Carvalho, O.; Person, K. Monthly Stream Flow Prediction in Pungwe River for Small Hydropower Plant Using Wavelet Method. *Int. J. Energy Power Eng.* **2015**, *4*, 280–286. [[CrossRef](#)]
38. Li, H.; Wang, Y.; Li, X. Mechanism and forecasting methods for severe droughts and floods in Songhua River Basin in China. *Chin. Geogr. Sci.* **2011**, *21*, 531–542. [[CrossRef](#)]
39. Szolgayova, E.; Parajka, J.; Blöschl, G.; Bucher, C. Long term variability of the Danube River flow and its relation to precipitation and air temperature. *J. Hydrol.* **2014**, *519*, 871–880. [[CrossRef](#)]
40. Li, A. Annual Runoff Forecasting Model based on Wavelet De-noising RSPA Method. *AISS* **2012**, *4*, 381–389.
41. Szolgayova, E.; Laaha, G.; Blöschl, G.; Bucher, C. Factors influencing long range dependence in streamflow of European rivers. *Hydrol. Process.* **2014**, *28*, 1573–1586. [[CrossRef](#)]
42. Armengol, J.; Sabater, S.; Vidal, A.; Sabater, F. Using the rescaled range analysis for the study of hydrological records: The River Ter as an example. *Oecol. Aquat.* **2012**, *10*, 21–34.
43. Wu, H.; Tang, D. Effect analysis on water diversion and short-term management of Heihe River based on rescaled range analysis method. *J. Arid Land Res. Environ.* **2007**, *21*, 27–30.
44. Shi, P.; Ma, X.; Chen, X.; Qu, S. Analysis of Variation Trends in Precipitation in an Upstream Catchment of Huai River. *Math. Probl. Eng.* **2013**, *2013*, 1262–1268. [[CrossRef](#)]

45. Svensson, C.; Brookshaw, A.; Scaife, A.A.; Bell, V.A.; Mackay, J.D.; Jackson, C.R. Long-range forecasts of UK winter hydrology. *Environ. Res. Lett.* **2015**, *10*, 10. [[CrossRef](#)]
46. Zhao, X.; Chen, X.; Huang, Q. Trend and long-term correlation characteristics analysis of runoff in upper Fenhe River basin. *Water Resour.* **2017**, *44*, 31–42. [[CrossRef](#)]
47. Jin, B. Application of Kendall Relevant Test of Order and Rescaled Range Analysis in the Analysis of Precipitation Variation Tendency. *Water Power* **2014**, *7*, 26–28.
48. Hamed, K.H. Improved finite-sample Hurst exponent estimates using rescaled range analysis. *Water Resour. Res.* **2007**, *43*, 797–809. [[CrossRef](#)]
49. Huang, J.; Zhang, J.; Zhang, Z.; Xu, C.Y. Spatial and temporal variations in rainfall erosivity during 1960–2005 in the Yangtze River basin. *Stoch. Environ. Res. Risk A* **2013**, *27*, 337–351. [[CrossRef](#)]
50. Nnaji, C.C. Time series analysis of monthly rainfall in Nigeria with emphasis on self-organized criticality. *J. Sci. Technol.* **2011**, *31*, 139–151. [[CrossRef](#)]
51. Gilmore, M.; Yu, C.X.; Rhodes, T.L.; Peebles, W.A. Investigation of rescaled range analysis, the Hurst exponent, and long-time correlations in plasma turbulence. *Phys. Plasmas* **2002**, *9*, 1312–1317. [[CrossRef](#)]
52. Rasheed, K.; Qian, B. Hurst exponent and financial market predictability. In Proceedings of the IASTED conference on Financial Engineering and Applications, Cambridge, MA, USA, 8–10 November 2004; pp. 203–209.
53. Bassingthwaite, J.B.; Raymond, G.M. Evaluating rescaled range analysis for time series. *Ann. Biomed. Eng.* **1994**, *22*, 432–444. [[CrossRef](#)] [[PubMed](#)]
54. Wallis, J.R.; Matalas, N.C. Small sample properties of H and K-Estimators of the Hurst coefficient h. *Water Resour. Res.* **1970**, *6*, 1583–1594. [[CrossRef](#)]
55. Kriřtoufek, L. Rescaled range analysis and detrended fluctuation analysis: Finite sample properties and confidence intervals. *AUCO Czech Econ. Rev.* **2010**, *4*, 315–330.
56. Barunik, J.; Kristoufek, L. On Hurst exponent estimation under heavy-tailed distributions. *Physica A* **2010**, *389*, 3844–3855. [[CrossRef](#)]
57. Mandelbrot, B.B. Statistical methodology for nonperiodic cycles: From the covariance to R/S analysis. In *Annals of Economic and Social Measurement*; NBER: New York, NY, USA, 1972; Volume 1, pp. 259–290.
58. North, C.P.; Halliwell, D.I. Bias in estimating fractal dimension with the rescaled-range (R/S) technique. *Math. Geol.* **1994**, *26*, 531–555. [[CrossRef](#)]
59. Meyer, L.D.; Wischmeier, W.H. Mathematical simulation of the process of soil erosion by water. *Am. Soc. Agric. Eng. Trans. ASAE* **1969**, *6*, 754–758.
60. Peters, E.E. *Chaos and Order in the Capital Markets: A new View of Cycles, Prices, and Market Volatility*; John Wiley & Sons: Hoboken, NJ, USA, 1996.
61. Lo, A.W. Long-Term Memory in Stock Market Prices. *Econometrica* **1989**, *59*, 1279–1313. [[CrossRef](#)]
62. Peters, E.E. Fractal Structure in the Capital Markets. *Financ. Anal. J.* **1989**, *45*, 32–37. [[CrossRef](#)]
63. Kamenshchikov, S.A. Transport catastrophe analysis as an alternative to a fractal description: Theory and application to financial crisis time series. *J. Chaos* **2014**, *1405*, 6990.
64. Yan, X.; Chang, Q.R.; Pan, J.P. Classification of Lou Soil in Chinese soil taxonomy in Guanzhong region. *Soil* **2004**, *36*, 318–322. (In Chinese)
65. Xu, X.Z.; Liu, D.Q.; Zhang, H.W.; Dong, Z.D.; Zhu, M.D. Laboratory rainfall simulation with controlled rainfall intensity and drainage. *J. Beijing. Fore. Univ.* **2006**, *28*, 52–58. (In Chinese)
66. Zhang, H.H.; Ta, N.; Zhang, H.; Dong, Y.; Tian, L.; Zhang, Q.F. Simulation of Runoff Hydraulics Parameters and Sediment Yield at Loess Tilled Slope. *J. Soil Water Conserv.* **2016**, *30*, 112–118. (In Chinese)

